Kupfer-type immunological synapse characteristics do not predict anti-brain tumor cytolytic T-cell function in vivo

J. Yang[a,b,c,d,1], N.S.R. Sanderson[a,b,c,d,1], K. Wawrowsky[a,b,c,d], M. Puntel[a], M.G. Castro[a,b,c,d], and P.R. Lowenstein[a,b,c,d,2]

[a]Board of Governors' Gene Therapeutics Research Institute, Department of Medicine and Department of Biomedical Sciences, Cedars-Sinai Medical Center, Los Angeles, CA 90048; Departments of [b]Medicine, and [c]Molecular and Medical Pharmacology, and [d]Jonsson Comprehensive Cancer Center, David Geffen School of Medicine, University of California Los Angeles, Los Angeles, CA 90024

Edited by Louis J. Ignarro, University of California Los Angeles David Geffen School of Medicine, Los Angeles, CA, and approved November 23, 2009 (received for review October 8, 2009)

To analyze the in vivo structure of antigen-specific immunological synapses during an effective immune response, we established brain tumors expressing the surrogate tumor antigen ovalbumin and labeled antigen-specific anti-glioma T cells using specific tetramers. Using these techniques, we determined that a significant number of antigen-specific T cells were localized to the brain tumor and surrounding brain tissue and a large percentage could be induced to express IFNγ when exposed to the specific ovalbumin-derived peptide epitope SIINFEKL. Detailed morphological analysis of T cells immunoreactive for tetramers in direct physical contact with tumor cells expressing ovalbumin indicated that the interface between T cells and target tumor cells displayed various morphologies, including Kupfer-type immunological synapses. Quantitative analysis of adjacent confocal optical sections was performed to determine if the higher frequency of antigen-specific antiglioma T cells present in animals that developed an effective antitumor immune response could be correlated with a specific immunological synaptic morphology. Detailed in vivo quantitative analysis failed to detect an increased proportion of immunological synapses displaying the characteristic Kupfer-type morphology in animals mounting a strong and effective antitumor immune response as compared with those experiencing a clinically ineffective response. We conclude that an effective cytolytic immune response is not dependent on an increased frequency of Kupfer-type immunological synapses between T cells and tumor cells.

anti-tumor immunity | brain tumors | immunotherapy

Interactions between effector T cells and target antigen-presenting cells (APCs) reveal a complex, spatiotemporally dynamic machinery at the intercellular interface. Immunological synapses (IS) were first characterized in the context of $CD4^+$ T-cell recognition of antigen presented by professional APCs. According to Monks et al. (1) and subsequently supported by many studies (2–9), upon ligation of the MHC/peptide complex by the T-cell receptor (TCR), several membrane-associated proteins, including the TCR complex and downstream kinases, become concentrated at the center of the contact interface, the central supramolecular activation complex (cSMAC), whereas others [e.g., lymphocyte function-associated antigen 1 (LFA-1), talin, and CD45] are excluded to form an outer concentric ring, the peripheral supramolecular activation complex (pSMAC) (1, 5, 10, 11). The structures displayed by $CD8^+$ cytotoxic T lymphocytes (CTL) as they interact with target cells share several important morphological and functional characteristics with the CD4/APC interaction (5, 12–18). Stinchcombe et al. (12) examined the synapses between primary mouse $CD8^+$ CTL and mouse mastocytoma targets, describing in detail the formation of cSMAC and pSMAC at the cytotoxic interface and how cytolytic granules are brought to a secretory subdomain within the cSMAC to focus cytotoxicity onto the targets (5, 12, 13). On the other hand, the need for stable IS for target-cell killing has been questioned by the observation that low levels of antigen on APCs stimulate Fas-mediated CTL killing without formation of stable Kupfer-type IS (19–21). Thus, the function of stable IS induced by higher antigen levels may be related more closely to perforin-mediated cytotoxicity (20) and/or cytokine secretion (15, 22). In addition to these in vitro studies, we and others have described SMACs in T cells in vivo, and the resulting cellular reorganization in "postsynaptic" target cells during the effector phase of an antiviral immune response (14–16, 25, 24) and in human brain tumors (17). Thus, although IS appear relevant to viral clearing and cytotoxicity in vitro and in vivo (14–17, 23, 24), their absolute requirement has been questioned (19–21, 25).

To study the role of Kupfer-type IS during an antigen-directed brain tumor immune response in vivo, we examined contacts between CTLs and targets in a well-characterized brain tumor model (26, 27), comparing 2 situations that differ in the effectiveness of the immune response. GL26 glioma tumors in the mouse brain do not elicit effective immunity and kill the hosts. However, they can be treated successfully with an immunostimulatory regimen of adenoviral (Ad) vectors encoding the cytokine Fms-like tyrosine kinase 3 ligand (Flt3L) and the conditionally cytotoxic transgene thymidine kinase (TK), inducing strong anti-tumor CTL response (26). To assess antigen specificity using MHC tetramers and cognate epitope-induced IFNγ production, GL26 glioma cells were engineered to express the antigen chicken ovalbumin.

We predicted that in treated animals, a higher proportion of IS would display typical Kupfer-type cSMAC/pSMAC IS morphology. Although antigen-specific antiglioma T cells were indeed enriched in tumors and brains of treated animals, these T cells displayed various synaptic morphologies, and there was no increased proportion of Kupfer-type IS in the animals mounting a strong immune response.

Results

FLt3L/TK Treatment Induces Effective Antitumor Immune Responses. The stable cell line GL26-cOVA expressed ovalbumin as assessed by immunoblotting (Fig. S1 *A* and *B*) or immunocytochemistry (Fig. S1 *C* and *D*), and brain tumors derived from these cells expressed ovalbumin as assessed by immunohistochemistry (Fig. S1 *E* and *F*). As has been described before using wild-type GL26 glioma cells (28) 20,000 GL26-cOVA cells implanted striatally

Author contributions: M.G.C. and P.R.L. designed research; .J.Y. N.S.R.S., and M.P. performed research; J.Y., N.S.R.S., K.W., M.G.C., and P.R.L. analyzed data; and J.Y., N.S.R.S., M.G.C., and P.R.L. wrote the paper.

The authors declare no conflict of interest.

This article is a PNAS Direct Submission.

[1]J.Y. and N.S.R.S. contributed equally to this work.

[2]To whom correspondence should be addressed at: Board of Governors' Gene Therapeutics Research Institute, Cedars-Sinai Medical Center, Davis Building, Room 5090, 8700 Beverly Boulevard, Los Angeles, CA 90048. E-mail: lowensteinp@cshs.org.

This article contains supporting information online at www.pnas.org/cgi/content/full/0911587107/DCSupplemental.

developed into a large tumor (Fig. 1*A* and Fig S1 *E* and *F*) that killed untreated hosts. Treatment with intratumoral injection of Ad.Flt3L and (Ad.TK) and systemic ganciclovir enabled ≈50% of the animals to clear the tumor and survive, whereas animals injected with saline died within 30 days of tumor implantation (Fig. 1*B*). Saline-injected animals killed at 27 days had large tumors occupying most of the striatum; treated animals had much smaller tumors (Fig. 1*A*).

Flow cytometry of lymphocytes labeled with anti-CD3ε or anti-CD8 antibodies and ovalbumin-derived peptide epitope SIINFEKL-H2K^b tetramers revealed more ovalbumin-specific T cells among the tumor-infiltrating cells in the treated animals than in controls (Fig. 1*C*), a difference that was not seen in the cervical lymph nodes or spleen (Fig. S2). Similarly, tumor-infiltrating CD3$^+$/CD8$^+$ cells from treated animals produced IFNγ in response to SIINFEKL at a higher frequency than did those from controls (Fig. 1*D*), and this difference was not observed in cells from the lymph nodes or spleen (Fig. S3). Total numbers of CD3ε immunoreactive cells were similar between groups (Fig. S4 *A* and *B*), although the tumors in treated animals displayed areas of very high T-cell density that were not observed in the controls (Fig. S4). Likewise, total numbers of brain-infiltrating CD4$^+$, CD8$^+$, and Foxp3$^+$ cells did not differ between treated and control animals, although in treated animals all these cell types accumulated most densely in a smaller area of the brain corresponding to the remnants of the treated tumor and the immediately surrounding brain (Fig. S5).

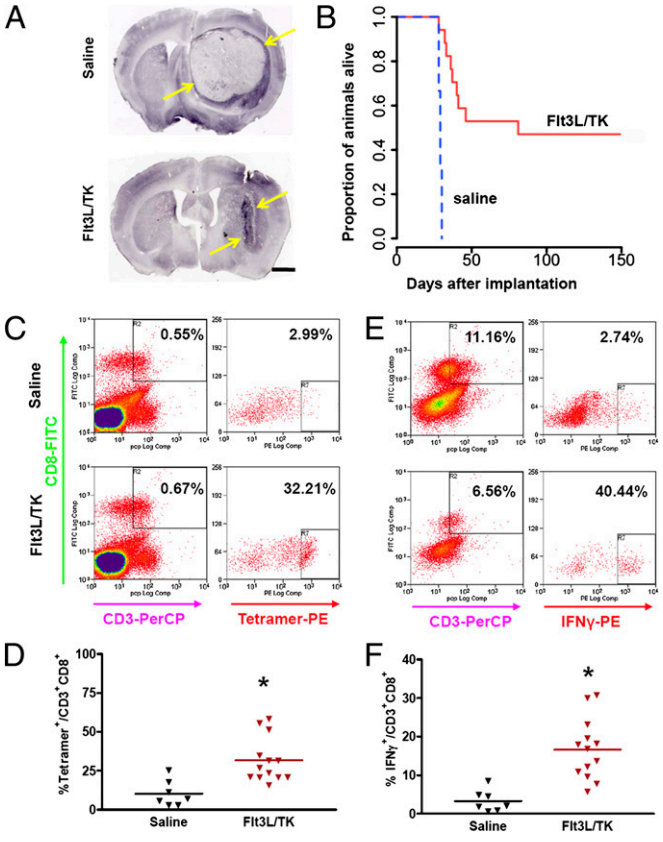

Fig. 1. Flt3L plus TK and ganciclovir treatment eliminates GL26 tumors and induces tumor infiltration of antigen-specific CD8+ T cells. (*A*) Comparison of GL26-cOVA tumors injected with saline (*Top*), or Flt3L/TK plus ganciclovir (*Bottom*). Brains were labeled using antibodies to CD8 to detect tumor-infiltrating T cells. Yellow arrows show extent of tumor at day 27. (Scale bar, 1 mm.) (*B*) Kaplan–Meier diagram comparing survival of Flt3L/TK-treated mice (solid red line) with saline-injected animals (dashed blue line). (*C*) Flow cytometry comparing frequencies of SIINFEKL-H2K^b tetramer-labeled CD3$^+$/CD8$^+$ tumor-infiltrating lymphocytes from saline-treated mice (*Upper plots*), and FLt3L/TK-treated mice (*Lower plots*). Cells were gated on CD8 and CD3 expression (*Left plots*), and tetramer binding was assessed within that population (*Right plots*, Y axis is side scatter). Percentages on each density plot are the proportion of cells falling within the zone defined by the small black rectangle. Each pair of density plots represents one animal. (*D*) The column scatter graph shows the percentage of CD8$^+$/CD3$^+$ cells that bind tetramer for 7 saline mice (black triangles) and 13 FLt3L/TK mice (brown triangles). Horizontal bars are group means; *, significantly greater than saline group ($P < 0.05$). (*E*) Density plots comparing the frequency of cells producing IFNγ in response to SIINFEKL stimulation in tumor-infiltrating lymphocytes from saline-treated mice (*Upper*) and from FLt3L/TK-treated mice (*Lower*). (*F*) The column scatter graph shows the percentage of CD8$^+$/CD3$^+$ cells that produce IFNγ in response to SIINFEKL stimulation for 7 saline-treated mice (black triangles) and 13 FLt3L/TK-treated mice (brown triangles). Horizontal bars are group means; *, greater than saline ($P < 0.05$).

Tumor-Infiltrating Cytotoxic T Lymphocytes Form Antigen-Specific Immunological Synapses with Tumor Cells. Antigen-specific CD8$^+$ cells were identified using in situ SIINFEKL-H2K^b tetramer labeling in GL26-cOVA tumors but never were identified in ovalbumin-negative, wild-type tumors (Fig. 2). In GL26-cOVA tumors, we observed T cells with patterns of tetramer and LFA-1 labeling that exhibited the SMAC pattern, i.e., depletion of LFA-1 at the concentration of tetramer (Fig. 3*A*). However, the converse also was observed—namely, colocalized enrichment of the 2 markers (Fig. 3*B*). To clarify the relationship between the formation of these structures and the process of CTL recognition of target cells, we repeated the tetramer and LFA-1 labeling process including an anti-ovalbumin antibody to identify antigenic targets. In these experiments, tetramer-labeled T cells were clearly identified interacting with ovalbumin-expressing tumor cells (Fig. 3*C*). Among tumor-attacking CTLs in contact with targets, some displayed the canonical Kupfer-type SMAC organization of tetramer concentration and LFA-1 depletion at the point of contact, with the region adjacent to the contact being relatively LFA-1 rich, but

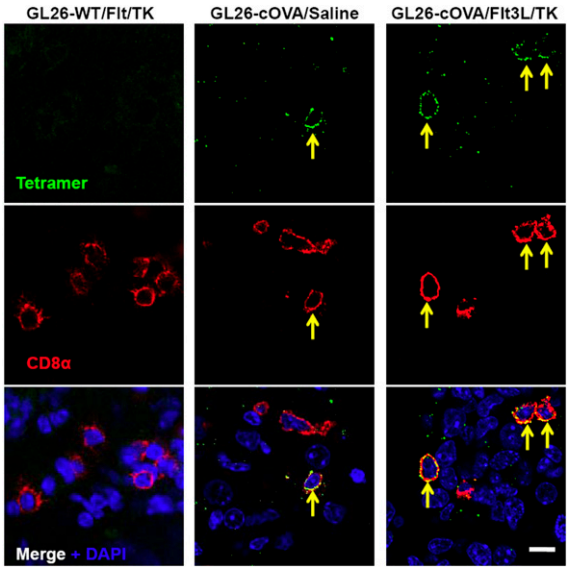

Fig. 2. Antigen-specific T cells infiltrate GL26-cOVA tumors in response to treatment. Immunofluorescent labeling using SIINFEKL-H2K^b tetramers (*Top row*) and anti-CD8 antibodies (*Middle row*) label ovalbumin-specific T cells (yellow arrows) infiltrating GL26-cOVA tumors. The Images in the left column are captured from a mouse implanted with wild-type GL26 cells and treated with Flt3L/TK. The images in the middle column are from a mouse implanted with GL26-cOVA cells and injected with saline. The images in the right column are from a mouse implanted with GL26-cOVA cells and treated with Flt3L/TK. Tetramer-binding T cells (indicated by yellow arrows) are found only in tumors derived from GL26-cOVA cells.(Scale bar, 10 μm.)

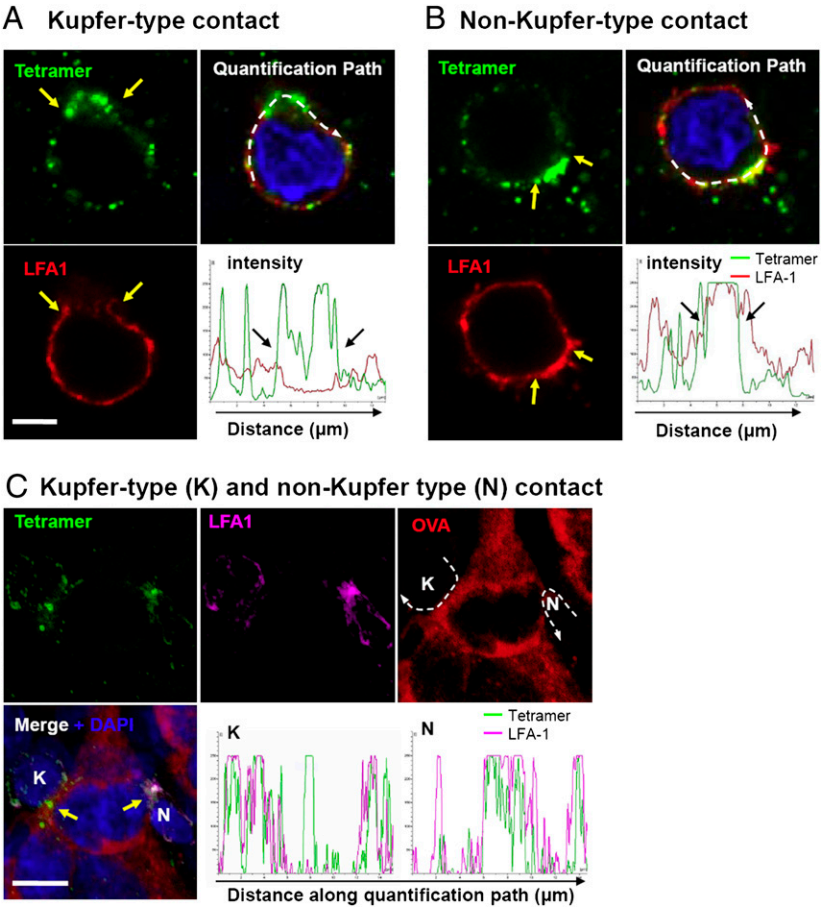

Fig. 3. Confocal Imaging of tumor-infiltrating, antigen (cOVA)-specific T cells identified using fluorescently labeled SIINFEK-H2K^b tetramers. (*A* and *B*) T cells from GL26-cOVA tumors of mice treated with Flt3L/TK and labeled with tetramers (green) and anti-LFA-1 antibodies (red). The yellow arrows demarcate an area of tetramer concentration, compatible with a polarized cSMAC. (Scale bar, 4 μm.) (*A*) A T cell with a distribution of tetramer and LFA-1 corresponding to the Kupfer-type cSMAC/pSMAC distribution (i.e., LFA-1 exclusion from the region of TCR concentration). (*B*) An alternative distribution (i.e., co-concentration of LFA-1 and TCR). The top right panels of *A* and *B* show the combination of LFA-1, tetramer, and DAPI (blue). The dashed white arrow marks the path along which the fluorescent intensity of tetramer and LFA-1 labeling was quantified. Results of this quantification are shown in the intensity plots in the bottom right of each figure, in which relative intensity (vertical axis) is plotted against distance along the quantification path. Marks on the horizontal axis represent 2 μm. (*C*) Micrographs from similar tissue in which, in addition to tetramers (green) and anti-LFA-1 antibodies (magenta), targets also were labeled using an anti-ovalbumin antibody (red). (Scale bar, 8 μm.) This image shows a single ovalbumin-expressing tumor cell (center) being attacked by two T cells. One of these T cells (marked "K") displays a Kupfer-type distribution of TCR concentration at the contact with the target, as marked by tetramer binding (solid yellow arrow), and LFA-1 exclusion from this area. The second T cell (marked "N") also shows tetramer accumulation at the contact, but LFA-1 is co-concentrated at the interface (i.e., an alternative to the pattern of the cSMAC/pSMAC model). Dashed white arrows in the top right (ovalbumin) panel show the paths along which the relative intensities of LFA-1 and tetramer were quantified, and these intensities are shown for each interface on the lower row (labeled "K" or "'N," respectively).

an alternative pattern (consisting of a co-concentration of LFA-1 and tetramer at the contact interface) was observed also. Fig. 3*C* shows a single ovalbumin-expressing tumor cell being attacked simultaneously by a CTL with Kupfer-type morphology (K, *Left*), and by a second CTL with both markers concentrated at the contact (N, *Right*). The degree of colocalization or mutual exclusion is shown in the intensity plots in Fig. 3, which show the relative fluorescent intensity associated with LFA-1 or tetramer, measured along a path drawn following the T-cell membrane, from one side of the contact to the other, for each contact. Both kinds of morphology and various intermediate morphologies were observed in both treated and control animals.

Distribution of Synapse Phenotype Is Not Correlated with Effectiveness of Immune Response. Following the observation of T-cell/target interfaces displaying Kupfer-type SMAC organization in both treated and control animals, we undertook a larger-scale, quantitative analysis of the morphologies of contacts. Tissue from the 2 groups was immunolabeled for ovalbumin (to identify target glioma cells), LFA-1 (to identify the pSMAC), and CD3ε, (to identify cSMAC). We then captured confocal stacks including >50 contacts from each group. Contacts were defined by polarized CD3ε at a T-cell/target interface and quantified. For each contact we identified the optical section that most centrally bisected T-cell/target cell contact; on this and adjacent sections (total, 3 sections per contact), we delineated the area at the center of the contact (representing the cSMAC) and the area to each side (the pSMAC) and recorded the mean fluorescent energy of the LFA-1 channel and the CD3ε channel. This procedure yielded a measure of the extent to which each contact was organized into Kupfer-type SMAC morphology, corresponding to high central and low peripheral CD3ε and low central and high peripheral LFA-1. Fig. 4*A* shows confocal images of a typical Kupfer-type synapse from an animal treated with Flt3L/TK and the quantitative data extracted from this synapse. Fig. 4*B* shows a synapse with the alternative distribution, i.e., co-concentration of the 2 markers at the contact interface. When we examined the contacts in tissue from saline-treated mice, we observed the same diversity of interfaces found in animals treated with Flt3L/TK. Fig. 5*A* shows confocal micrographs and quantitative data from a Kupfer-type synapse found in a saline-treated animal, and Fig. 5*B* shows a synapse with both CD3ε and LFA-1 concentrated at the interface.

We predicted that the effective antitumor immune response in animals treated with Flt3L/TK would be reflected in a higher frequency of IS displaying canonical Kupfer-type morphology. Averages from three sections per contact were plotted as a ratio of LFA-1 intensity in the cSMAC to LFA-1 intensity in the pSMAC to yield distributions of the preponderance of Kupfer-type morphology (Fig. 6*A*). These data also were evaluated with respect to CD3ε concentration in the IS, with LFA-1–depleted cSMAC in 1 group (Kupfer-type IS; Fig. 6*B*) and LFA-1–enriched cSMAC in a second group (non–Kupfer-type IS; Fig. 6*B*) to determine whether polarization of CD3ε correlated with LFA-1 distribution. Distributions were indistinguishable between groups (Fig. 6). To determine whether antigen-specific T cells form comparable IS with target tumor cells, we implanted GL26-cOVA or GL26 cells into RAG1$^{-/-}$ mice and treated the tumors with Flt3L/TK. Two days later, we transplanted 1×10^7 OT-I splenocytes into treated mice. Nine days later, animals were perfused, and tumors were analyzed for the presence of OT-I cells. OT-I cells infiltrated only tumors expressing ovalbumin (Fig. S6). Polarization of CD3ε (Fig. S7 *A* and *B*), and IFNγ at contacts (Fig. S7*C*) suggested the formation of IS; unexpectedly low levels of LFA-1 precluded complete characterization.

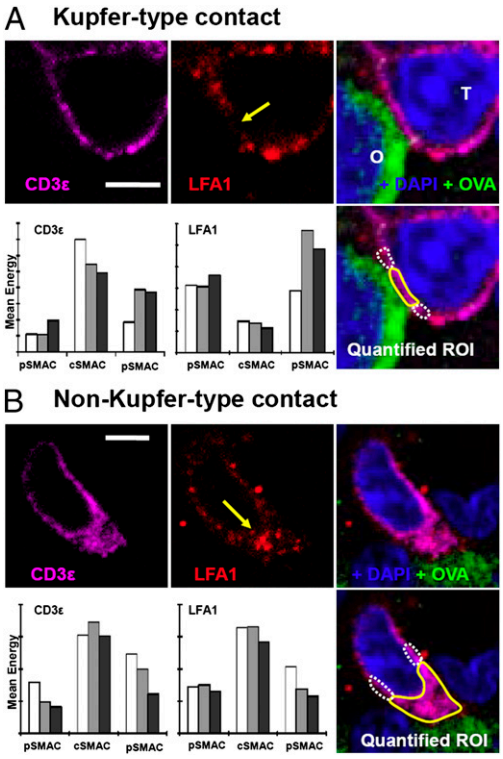

Fig. 4. Confocal micrographs of T cells and targets from GL26-cOVA tumors in mice injected with Flt3L/TK. (*A*) A synapse that exhibits the Kupfer-type SMAC organization. (*B*) An interface with an alternative distribution (i.e., co-concentration of LFA-1 and CD3ε). (Scale bars, 5 μm.) The left and middle images in the top rows show the distribution of CD3ε (magenta) and LFA-1 (red), respectively. In the LFA-1 image, a yellow arrow shows the point at which the T cell contacts the target. The right image in the top row shows the combination of these channels together with immunolabeling for ovalbumin (green) and DAPI (blue). Here the T cell is marked "T," and the ovalbumin-expressing target is marked "O." On the bottom right is another merged image in which the areas corresponding to the cSMACs are marked with solid yellow lines and the pSMACs with broken white lines. In these regions of interest, mean fluorescent density was recorded for LFA-1 and CD3ε on three adjacent sections through the T-cell/target cell contact; these data are shown in the bar charts (*Bottom rows left and middle*). The light gray bar is the measurement from the section centrally bisecting the contact, and the white and dark gray bars are from the adjacent sections. The bar chart at the left of the bottom row shows measurements of CD3ε, and the bar chart in the middle of the bottom row shows LFA-1. The quantification and statistical analysis of all contacts studied are shown in Fig. 6.

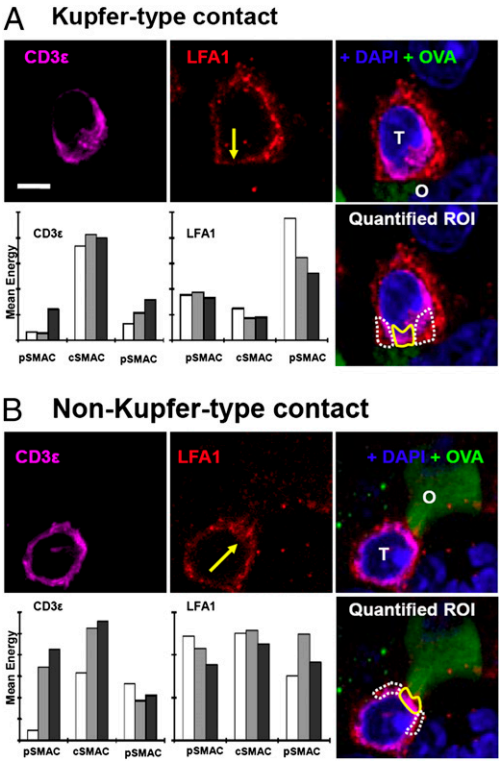

Fig. 5. Confocal micrographs of T cells and targets from GL26-cOVA tumors in mice injected with saline. (*A*) A synapse that exhibits the Kupfer-type SMAC organization. (*B*) An interface with an alternative distribution (i.e., co-concentration of LFA-1 and CD3ε at the center of the interface). (Scale bar, 5 μm.) Left and middle images in the top rows show CD3ε (magenta) and LFA-1 (red). In the LFA-1 image, a yellow arrow indicates the point at which the T cell contacts the target. The right images in the top rows show the combination of these channels together with immunolabeling for ovalbumin (green) and DAPI (blue). In these images, the T cell is marked "T," and the ovalbumin-expressing target is marked "O." The bottom right panels show another merged image in which the areas corresponding to the cSMACs are marked with solid yellow lines and the pSMACs with broken white lines. In these regions of interest, mean fluorescent density was recorded for LFA-1 and CD3ε on three adjacent sections through the T-cell/target cell contact, and these data are shown in the bar charts in left and middle panels of the bottom rows. The light gray bar is the measurement from the section centrally bisecting the contact, and the white and dark gray bars are from the adjacent sections. The bar charts on the left of the bottom rows show measurements of CD3ε, and the bar charts in the middle of the bottom rows show LFA-1. The quantification and statistical analysis of all contacts studied are shown in Fig. 6.

Discussion

The morphology of IS would be predicted to reflect the therapeutic efficiency of the antitumoral immune response. In our experiments treatment-induced therapeutic efficiency was reflected in increased survival, increased tumor infiltration of glioma antigen-specific T cells, and an increase in their IFNγ production in response to antigen challenge. A higher proportion of T-cell/glioma contacts displaying the characteristic cSMAC/pSMAC morphology of Kupfer-type IS was expected. However, treatment efficacy failed to correlate with an increase in the proportion of Kupfer-type IS between T cells and glioma cells detected in treated animals.

In vitro studies suggest that IS underpin intercellular immune interactions. We tested the relevance of IS to in vivo brain tumor immune responses. In culture, $CD8^+$ CTL form SMACs only during contact with targets displaying the appropriate antigenic epitopes (3, 5, 19), although the level of antigen displayed by MHC, the concentration of adhesion molecules, and the nature of the epitopes and APC influence the type of junctions formed (6, 15, 30–33). Because lysis by CTLs depends on antigen recognition and cell-to-cell contact, it has been proposed that SMACs are necessary for effective and selective lysis of targets to occur (i.e., to restrict cytotoxic consequences to the appropriate target cells) (4, 12, 13, 15). The amount of antigen required to activate CTL cytolysis in vitro, however, is less than that required to form stable IS, suggesting that at least some forms of $CD8^+$ T-cell–mediated cytotoxicity do not require stable IS (20, 37, 38). It is possible that Fas-mediated cytotoxicity, lytic-granule–mediated cytotoxicity, and cytokine secretion may each be accompanied by differential morphological synaptic specializations (4, 6, 12, 15, 19–22, 25, 34–36).

To demonstrate the necessity of IS for immune-mediated tumor cytotoxicity in vivo is more challenging; within the tumor microenvironment T cells simultaneously may contact several cells, which may display appropriate antigenic epitopes. Nevertheless, Kupfer-

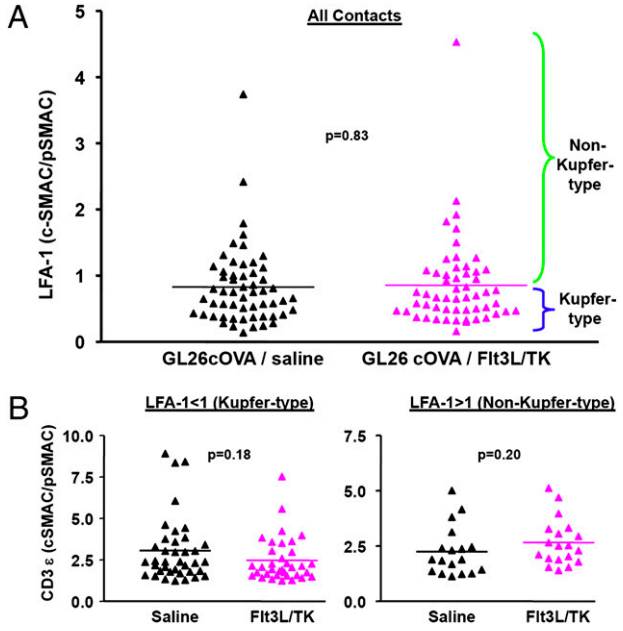

Fig. 6. Quantitative analysis of the frequency of T-cell/glioma cell contacts displaying various distributions of LFA-1 and CD3ε in FLt3L/TK-treated mice (pink triangles), or in control mice injected with saline (black triangles). This figure illustrates detailed quantitative analysis of 111 IS interfaces in which the distribution of CD3ε and LFA-1 at each interface was quantitated in at least three adjacent optical sections in the three regions of interest (as in Figs. 4 and 5). All interfaces were identified by CD3ε strongly polarized toward ovalbumin-expressing glioma cells and were colabeled with LFA-1. (*A*) Each triangle represents one immunological synapse, with the degree of LFA-1 focusing (i.e., the ratio of LFA-1 in the cSMAC to LFA-1 in the pSMAC) displayed on the vertical axis. IS conforming to the Kupfer-type cSMAC pattern should fall at the bottom of this distribution (indicated by the blue bracket at the right of the figure). IS at the top of the distribution show LFA-1 which tends to colocalize with CD3ε at the interface (green bracket). IS from saline-injected mice are in the left column, and those from Flt3L/TK-treated mice are in the right column. This graph indicates that there is a wide range of LFA-1 distribution at IS interfaces, but there is no difference between animals mounting a therapeutically effective immune response (Flt3L/TK), and those that do not (saline). (*B*) The total population of IS was divided into two subsets: On the left are the IS in which LFA-1 was depleted at the contact site (i.e., the ratio of LFA-1 in the cSMAC to LFA-1 in the pSMAC is < unity, displaying the pattern of Kupfer-type IS). On the right are those in which LFA-1 was enriched at the contact. The vertical axes represent the degree to which the CD3ε was concentrated in the cSMAC. These two figures indicate that the degree of CD3ε polarization toward the target tumor cells did not vary with the segregation pattern of LFA-1. The entire experiment was repeated twice, with similar results. Differences between groups were analyzed by repeated-measures ANOVA, and resulting *P* values are shown. Differences between groups were not statistically significant.

type IS have been described during antiviral and antitumor immune responses in vivo in animals and humans (14–17, 23, 24, 37–39).

The causal relevance for IS was studied to assess (*i*) the antigen specificity of IS during an antitumoral immune response and (*ii*) whether the morphology of IS would reflect the therapeutic efficiency of the in vivo immune response. A tumor model was developed in which tumor cells express the model antigen ovalbumin to facilitate the assessment of the antigen specificity of the interactions in vivo. We found that tetramer-positive $CD8^+$ T cells indeed participated in the formation of Kupfer-type IS with target tumor cells expressing the cognate antigen. We examined CTLs infiltrating syngeneic glioma tumors treated with Ad.FLt3L and Ad.TK followed by ganciclovir and in untreated tumors. The advantage of this comparison is that a large number of previous studies have described the induction of an effective immune response in the former and its absence from the latter (26–28, 40). This $CD8^+$ T-cell–dependent immune response is thought to be initiated by dendritic cells activated by the combination of Flt3L and Toll-like receptor 2 ligands released from dying tumor cells (28).

In view of the quantitative difference between treated mice and controls, we gathered detailed CD3ε and LFA-1 distribution data from a large number of contacts between T cells and targets from both groups. Our expectation was that, even if SMACs were present in both groups, examination of a large body of data would reveal an increased occurrence of Kupfer-type IS commensurate with other measures of immune response strength, such as the frequency of SIINFEKL-specific IFNγ-secreting T cells. This expectation was not borne out. Although the immune response was substantially stronger in treated animals, there was no increase in the frequency of Kupfer-type IS.

A number of limitations of the strategy employed here must be considered in interpreting the result that the frequency and characteristics of Kupfer-type IS did not reflect the strength of the immune response. First, we wished to compare IS between animals that differed in the clinical effectiveness of their antitumor immune response rather than performing our comparison of IS in an all-or-none paradigm. However, we believe an all-or-none paradigm (see Figs. S6 and S7) is less informative, because with no T cells in the control animals, it becomes impossible to correlate and quantify differences of IS with strength of immune responses. Therefore, we believe the paradigm used represents a reasonable tradeoff to explore the physiological role of IS in a relevant model of immune-mediated tumor rejection.

A second caveat is that we selected contacts with polarized CD3ε between T cells and OVA-expressing tumor cells in both groups; this selection was necessary as an indication of contact formation between T cells and targets. The selection of cells with polarized CD3ε might have biased our study toward T cells already forming IS in both groups. Because there were similar numbers of T cells in both groups, we expected that the higher proportion of activated antigen-specific T cells in the treated group would be reflected in a higher proportion of effective cytolytic interactions and a higher proportion of Kupfer-type IS, if these structures correlate with the strength of the in vivo immune response. A third caveat is that the quantitative morphological analysis described here was limited to CD3ε and LFA-1 distribution. These molecules were chosen because of the wealth of studies describing and characterizing their involvement in the cSMAC and pSMAC of typical Kupfer-type synapse. Future studies could focus attention on whether the distribution of other synapse-associated molecules provides a better indication of the strength of the anti-brain tumor immune response in vivo. Equally, it is likely that dynamic imaging studies will be necessary to address the function of IS in vivo.

In summary, the results of our studies demonstrate the existence of Kupfer-type antigen-specific IS, accompanied by a wide range of other synaptic morphologies in vivo, during immune-mediated elimination of brain tumors. This same continuum of synaptic morphologies was detected both when antigen-specific T cells engaging tumor cells were labeled with specific tetramers and when we carefully characterized the structure of IS through a serially quantitative assessment of the distribution of CD3ε and LFA-1. Elucidating the role of Kupfer-type IS during ongoing in vivo immune responses and the precise morphological correlates of CTL cytotoxicity may require the development of novel imaging techniques to detect simultaneously the morphology and function of T cells by optical means in live animals. Nevertheless, the weight of available data supports the hypothesis that an effective T-cell immune response is mediated by a range of morphological synaptic specializations rather than relying solely on the formation of Kupfer-type IS.

Materials and Methods

Animals, Tumor Implantation, Survival Studies, and Immunohistochemistry. Animal experiments complied with Cedars-Sinai Medical Center's Institutional Animal Care and Use Committee. C57BL/6 mice were implanted with GL26-cOVA or GL26 cells and treated with Ad.Flt3L/TK or saline as described in more detail in *SI Materials and Methods* and in ref.30. For the survival study, 3 animals were injected intratumorally with saline, and 17 animals were injected with Ad.Flt3L/TK and given ganciclovir. Immunohistochemical labeling of ovalbumin, CD3ε, and LFA-1 for quantitative studies was repeated in 2 independent experiments which yielded similar results. C57BL/6 mice were implanted with GL26-cOVA and treated 17 days later with Ad.Flt3L/TK (n = 7) or saline (n = 5); 29 days after tumor implantation, animals were perfused with oxygenated Tyrode's solution, followed by 4% paraformaldehyde, and brains postfixed for 24–48 h. 50 μm coronal sections were vibratome cut, immunolabeled, and visualized using immunofluorescence or peroxidase histochemistry using rat anti-mouse CD8, Syrian hamster anti-mouse CD3ε (1:500) (BD Biosciences), rat anti-mouse LFA-1, and rabbit anti-ovalbumin, as described in detail in *SI Materials and Methods* and refs. 15, 28, and 40.

In Situ Tetramer Labeling. At 29 days after tumor implantation, mice were anesthetized and perfused transcardially with oxygenated Tyrode's solution. Brains were removed, fixed in 2% paraformaldehyde in PBS at room temperature for 30 min, stored overnight in PBS at 4 °C, and embedded in 4% low-melt agarose in PBS. 200 μm sections were cut in ice-cold PBS and stained free-floating at 4 °C. Antigen-specific T cells were labeled using allophycocyanin-conjugated SIINFEKL-H-2K^b MHC tetramers (1:200) (Beckman Inc.); because of the rapid bleaching of allophycocyanin, we used rabbit anti-allophycocyanin antibodies (Novus Biologicals) 1:500 and goat anti-rabbit conjugated to Alexa 488 (1:500) to visualize tetramers. Multiple labeling of tetramer-stained sections proceeded as follows: rat anti-CD8 (1:5000) (Serotec), or rat anti-LFA-1 (1:500) (BD Bioscience) were detected with Alexa 594-conjugated goat anti-rat (1:500) (Invitrogen) or Alexa 546-conjugated goat anti-rat (1:500) (Invitrogen). In experiments labeling both tetramers and ovalbumin simultaneously, tetramers were visualized with Dylight 488 goat anti-rabbit Fab fragments (1:50) (Jackson). Ovalbumin was detected with specific rabbit antibodies (1:500) (Abcam), following blocking with unconjugated goat anti-rabbit Fab (1:100) (Jackson), and was visualized with goat anti-rabbit Alexa 594 (1:500) (Invitrogen). The use of unconjugated goat anti-rabbit Fab was optimized to avoid cross-labeling, and controls were included in each experiment.

Confocal Microscopy, Analysis, and Statistics. Subcellular distribution of LFA-1 and CD3ε was analyzed at 136 contacts between T cells and ovalbumin-expressing glioma cells in brain sections from 12 mice (7 in the first experiment and 5 in the second). Sections were examined with a Leica TCS-SP2 confocal microscope with the PlanAPO 63× 1.4 NA oil objective and LCS Confocal Software (Leica Microsystems) (14–16). A potential contact interface was defined as the junction between a T cell and an ovalbumin-positive glioma cell in which CD3ε was strongly polarized towards the interface and CD3ε and LFA-1 were both present at the interface in at least 3 sequential optical sections. To assess the extent to which the 2 proteins were distributed in the pattern characteristic of the Kupfer-type synapse, mean fluorescence density was measured in 3 adjacent regions on the T-cell side of the contact, 1 in the center and 1 on each side, in each of 3 successive sections. The overall difference between Ad.Flt3L/TK-treated and saline groups in the degree of LFA-1 exclusion from the cSMAC (Fig. 6*A*) or the polarization of CD3 towards the cSMAC (Fig. 6*B*) was compared by repeated-measures ANOVA, with treatment group as the between-subjects variable, using NCSS software. For quantitative analysis of the distribution of tetramer and LFA-1 staining across the synaptic interface, the relative fluorescent intensity was measured along a path as illustrated in Fig 3.

ACKNOWLEDGMENTS. We thank Drs. Melmed, Greene, and Fine for enthusiastic support. Our work was supported in part by NIH/NINDS Grants 1R01NS44556.01, Minority Suppl NS445561.01; 1R21NSO54143.01; 1UO1NS052465.01, 1RO3TW006273-01; and 1RO1NS 057711 to M.G.C.; NIH/NINDS Grants 1RO1NS 054193.01; RO1 NS42893.01, U54 NS045309-01, and 1R21NS047298-01 to P.R.L.; The Bram and Elaine Goldsmith and the Medallions Group Endowed Chairs in Gene Therapeutics to P.R.L. and M.G.C., respectively, The Linda Tallen & David Paul Kane Foundation Annual Fellowship, and the Board of Governors at Cedars-Sinai Medical Center.

1. Monks CR, Freiberg BA, Kupfer H, Sciaky N, Kupfer A (1998) Three-dimensional segregation of supramolecular activation clusters in T cells. *Nature* 395:82–86.
2. Huse M, Quann EJ, Davis MM (2008) Shouts, whispers and the kiss of death: Directional secretion in T cells. *Nat Immunol* 9:1105–1111.
3. Dustin ML (2009) The cellular context of T cell signaling. *Immunity* 30:482–492.
4. Stinchcombe JC, Griffiths GM (2007) Secretory mechanisms in cell-mediated cytotoxicity. *Annu Rev Cell Dev Biol* 23:495–517.
5. Grakoui A, et al. (1999) The immunological synapse: A molecular machine controlling T cell activation. *Science* 285:221–227.
6. Trautmann A, Valitutti S (2003) The diversity of immunological synapses. *Curr Opin Immunol* 15:249–254.
7. Lee KH, et al. (2003) The immunological synapse balances T cell receptor signaling and degradation. *Science* 302:1218–1222.
8. Stoll S, Delon J, Brotz TM, Germain RN (2002) Dynamic imaging of T cell-dendritic cell interactions in lymph nodes. *Science* 296:1873–1876.
9. Cemerski S, Shaw A (2006) Immune synapses in T-cell activation. *Curr Opin Immunol* 18:298–304.
10. Friedl P, den Boer AT, Gunzer M (2005) Tuning immune responses: Diversity and adaptation of the immunological synapse. *Nat Rev Immunol* 5:532–545.
11. Kupfer A, Kupfer H (2003) Imaging immune cell interactions and functions: SMACs and the immunological synapse. *Semin Immunol* 15:295–300.
12. Stinchcombe JC, Bossi G, Booth S, Griffiths GM (2001) The immunological synapse of CTL contains a secretory domain and membrane bridges. *Immunity* 15:751–761.
13. Stinchcombe JC, Majorovits E, Bossi G, Fuller S, Griffiths GM (2006) Centrosome polarization delivers secretory granules to the immunological synapse. *Nature* 443:462–465.
14. Barcia C, et al. (2006) In vivo mature immunological synapses forming SMACs mediate clearance of virally infected astrocytes from the brain. *J Exp Med* 203:2095–2107.
15. Barcia C, et al. (2008) In vivo polarization of IFN-γ at Kupfer and non-Kupfer immunological synapses during the clearance of virally infected brain cells. *J Immunol* 180:1344–1352.
16. Barcia C, et al. (2008) T cells' immunological synapses induce polarization of brain astrocytes in vivo and in vitro: A novel astrocyte response mechanism to cellular injury. *PLoS One* 3:e2977.
17. Barcia C, et al. (2009) Infiltrating CTLs in human glioblastoma establish immunological synapses with tumorigenic cells. *Am J Pathol* 175:786–798.
18. Beal AM, et al. (2008) Protein kinase C theta regulates stability of the peripheral adhesion ring junction and contributes to the sensitivity of target cell lysis by CTL. *J Immunol* 181:4815–4824.
19. Purbhoo MA, Irvine DJ, Huppa JB, Davis MM (2004) T cell killing does not require the formation of a stable mature immunological synapse. *Nat Immunol* 5:524–530.
20. Huppa JB, Davis MM (2003) T-cell-antigen recognition and the immunological synapse. *Nat Rev Immunol* 3:973–983.
21. Huppa JB, Gleimer M, Sumen C, Davis MM (2003) Continuous T cell receptor signaling required for synapse maintenance and full effector potential. *Nat Immunol* 4:749–755.
22. Wiedemann A, Depoil D, Faroudi M, Valitutti S (2006) Cytotoxic T lymphocytes kill multiple targets simultaneously via spatiotemporal uncoupling of lytic and stimulatory synapses. *Proc Natl Acad Sci USA* 103:10985–10990.
23. McGavern DB, Christen U, Oldstone MB (2002) Molecular anatomy of antigen-specific CD8(+) T cell engagement and synapse formation in vivo. *Nat Immunol* 3:918–925.
24. Khanna KM, Bonneau RH, Kinchington PR, Hendricks RL (2003) Herpes simplex virus-specific memory CD8+ T cells are selectively activated and retained in latently infected sensory ganglia. *Immunity* 18:593–603.
25. Faroudi M, et al. (2003) Lytic versus stimulatory synapse in cytotoxic T lymphocyte/target cell interaction: Manifestation of a dual activation threshold. *Proc Natl Acad Sci USA* 100:14145–14150.
26. King GD, et al. (2008) Flt3L and TK gene therapy eradicate multifocal glioma in a syngeneic glioblastoma model. *Neuro-oncol* 10:19–31.
27. Curtin JF, et al. (2006) Fms-like tyrosine kinase 3 ligand recruits plasmacytoid dendritic cells to the brain. *J Immunol* 176:3566–3577.
28. Curtin JF, et al. (2009) HMGB1 mediates endogenous TLR2 activation and brain tumor regression. *PLoS Med* 6:e10.
29. Lee KH, et al. (2002) T cell receptor signaling precedes immunological synapse formation. *Science* 295:1539–1542.
30. Somersalo K, et al. (2004) Cytotoxic T lymphocytes form an antigen-independent ring junction. *J Clin Invest* 113:49–57.
31. Brossard C, et al. (2005) Multifocal structure of the T cell-dendritic cell synapse. *Eur J Immunol* 35:1741–1753.
32. Revy P, Sospedra M, Barbour B, Trautmann A (2001) Functional antigen-independent synapses formed between T cells and dendritic cells. *Nat Immunol* 2:925–931.
33. O'Keefe JP, Gajewski TF (2005) Cutting edge: Cytotoxic granule polarization and cytolysis can occur without central supramolecular activation cluster formation in CD8+ effector T cells. *J Immunol* 175:5581–5585.
34. Krogsgaard M, Huppa JB, Purbhoo MA, Davis MM (2003) Linking molecular and cellular events in T-cell activation and synapse formation. *Semin Immunol* 15:307–315.
35. Caramalho, I., et al. (2008) Visualizing CTL/melanoma cell interactions: Multiple hits must be delivered for tumor cell annihilation. *J Cell Mol Med* .
36. Depoil D, et al. (2005) Immunological synapses are versatile structures enabling selective T cell polarization. *Immunity* 22:185–194.
37. Kim JV, Kang SS, Dustin ML, McGavern DB (2009) Myelomonocytic cell recruitment causes fatal CNS vascular injury during acute viral meningitis. *Nature* 457:191–195.
38. Kivisäkk P, et al. (2009) Localizing central nervous system immune surveillance: Meningeal antigen-presenting cells activate T cells during experimental autoimmune encephalomyelitis. *Ann Neurol* 65:457–469.
39. Bauer J, et al. (2007) Astrocytes are a specific immunological target in Rasmussen's encephalitis. *Ann Neurol* 62:67–80.
40. Dewey RA, et al. (1999) Chronic brain inflammation and persistent herpes simplex virus 1 thymidine kinase expression in survivors of syngeneic glioma treated by adenovirus-mediated gene therapy: Implications for clinical trials. *Nat Med* 5:1256–1263.